

---

Article

Not peer-reviewed version

---

# Design of Green $\text{TiO}_2$ -Based Semiconductors for Microplastic and Nanoplastics Photocatalytic Degradation

---

[Aranza Denisse Vital-Grappin](#) , [Maria Camila Ariza-Tarazona](#) , Isaac Sandoval ,  
Cesar Abraham Rojas-Guerrero , [Juan Francisco Villarreal-Chiu](#) , [Erika Iveth Cedillo-González](#) \*

Posted Date: 30 January 2023

doi: [10.20944/preprints202301.0544.v1](https://doi.org/10.20944/preprints202301.0544.v1)

Keywords: microplastics; nanoplastics;  $\text{TiO}_2$ ; crystallinity; film; photocatalysis; degradation; mitigation; microplastic pollution.



Preprints.org is a free multidiscipline platform providing preprint service that is dedicated to making early versions of research outputs permanently available and citable. Preprints posted at Preprints.org appear in Web of Science, Crossref, Google Scholar, Scilit, Europe PMC.

Copyright: This is an open access article distributed under the Creative Commons Attribution License which permits unrestricted use, distribution, and reproduction in any medium, provided the original work is properly cited.

Disclaimer/Publisher's Note: The statements, opinions, and data contained in all publications are solely those of the individual author(s) and contributor(s) and not of MDPI and/or the editor(s). MDPI and/or the editor(s) disclaim responsibility for any injury to people or property resulting from any ideas, methods, instructions, or products referred to in the content.

## Article

# Design of Green $\text{TiO}_2$ -Based Semiconductors for Microplastic and Nanoplastics Photocatalytic Degradation

Aranza Denisse Vital-Grappin <sup>1</sup>, Maria Camila Ariza-Tarazona <sup>2</sup>, Isaac Sandoval <sup>1</sup>, Cesar Abraham Rojas-Guerrero <sup>1</sup>, Juan Francisco Villarreal-Chiu <sup>1,3</sup> and Erika Iveth Cedillo-González <sup>1,2,4,\*</sup>

<sup>1</sup> Universidad Autónoma de Nuevo León, Facultad de Ciencias Químicas, Av. Universidad S/N Ciudad Universitaria, San Nicolás de los Garza, Nuevo León, 66455, Mexico; vital.grappin@gmail.com (A.D.V.-G.); lascienzapergaia@gmail.com (I.S.); csr25cesar@gmail.com (C.A.R.-G.); juan.villarrealch@uanl.edu.mx (J.F.V.-C.)

<sup>2</sup> Department of Engineering “Enzo Ferrari”, University of Modena and Reggio Emilia, Via P. Vivarelli 10/1, 41125 Modena, Italy; mariacamila.arizatarazona@unimore.it

<sup>3</sup> Centro de Investigación en Biotecnología y Nanotecnología (CIByN), Facultad de Ciencias Químicas, Universidad Autónoma de Nuevo León. Parque de Investigación e Innovación Tecnológica, Km. 10 autopista al Aeropuerto Internacional Mariano Escobedo, Apodaca 66629, Nuevo León, Mexico

<sup>4</sup> National Interuniversity Consortium of Materials Science and Technology (INSTM), Via G. Giusti 9, Florence 50121, Italy.

\* Correspondence: ecedillo@unimore.it; Tel.: +39-0592056218

**Abstract:** Microplastics (MPs) and nanoplastics (NPs) are distributed and transferred among the four major environmental compartments (air, water, soil, and biota) and have been already found in humans, making crucial to develop remediation technologies to tackle this kind of pollution. Photocatalysis can be used to eliminate MPs present in contaminated wastewater effluents before their discharge into waterbodies. In this work, several green  $\text{TiO}_2$ -based semiconductors were prepared using the extrapallial fluid (EPF) of *Mytilus edulis* sea water mussels as doping precursor. The semiconductors were then used as films or powders to photocatalytically degrade polystyrene (PS) NPs and MPs and polyethylene (PE) MPs. It was found that the obtention of green  $\text{TiO}_2$ -based semiconductors with good characteristics for photocatalytic purposes (anatase crystalline phase, presence of porosity, activity in visible light and high surface area) seems not enough to achieve high degradation efficiency. The operational conditions of the reaction system should be also taken into account. For instance, the convenience of using semiconductors in the form of films can be overcome by their limited exposed surface area or the null adsorption of the semiconductor in the MPs particles. Additionally, crystallinity of the semiconductor can be a more determinant factor to take into account when performing photocatalysis of MPs.

**Keywords:** microplastics; nanoplastics;  $\text{TiO}_2$ ; crystallinity; film; photocatalysis; degradation; mitigation; microplastic pollution.

## 1. Introduction

By 2013, 268,950 tonnes of plastic were found on the surface of the ocean [1]. Gall et al. (2015) report, in a study of 340 articles, that they found 693 organisms and marine species have had contact with marine trash, 92% of the contact reported was with plastic debris [2]. One of the fundamental issues with plastics in marine ecosystems is their ingestion and entanglement [3]. In recent years, microplastics (MPs) and nanoplastics (NP) have gained the scientific community's attention. MPs are defined as plastic with sizes between 1  $\mu\text{m}$  and 5 mm long, nanoplastics are defined as plastics smaller than 1  $\mu\text{m}$  [4]. Recent studies have reported that MPs and NPs have been found in biota [5,6], table salt [7], drinking water [8], milk [9], seafood [10], human bloodstream [11], human placenta [12],

and human stool [13], among others. Additionally, MPs can transport persistent organic pollutants (POPs). Due to their intrinsic properties, such as specific surface area, crystallinity, hydrophobicity and polarity and the POPs' hydrophobicity and dissociative forms, these organic pollutants tend to adsorb in MPs [14]. Additionally, MPs can sorb heavy metals [15]. Thus, MPs work as a vector for POPs and heavy metal transporting into organisms. For instance, Liao et al. (2019) reported Cr bioaccessibility in the human digestive system through MPs [16,17].

Water bodies have become contaminated with microplastics from domestic sources, pharmaceutical products, ships, research facilities, and maritime and wastewater treatment facilities. Wastewater treatment plants (WWTPs) are a source of MPs to aquatic systems due to unfitted systems for MPs removal and terrestrial systems because of MPs capture in the sludge that is afterwards used for fertilization [18]. Thus, a feasible approach for effectively eliminating the MPs before their incorporation into water bodies would be pollutant elimination in WWTPs. Different technologies have been studied for addressing MPs remediation in aquatic systems, namely, membrane technology, coagulation and flocculation, nanomaterials, bacterial biodegradation, electrocoagulation and advanced oxidation processes (AOPs) [19]. AOPs are an attractive solution to MPs remediation owing to the possibility of MPs mineralization [20].

AOPs include photochemical oxidation [21], ozonation [22], electrochemical oxidation [23], catalytic oxidation [24] and photocatalytic oxidation [25]. Photocatalytic degradation is a viable solution for MPs degradation, as it can be adapted as a tertiary treatment in a WWTP, as well as allowing the mineralization of microplastics to  $\text{CO}_2$  and  $\text{H}_2\text{O}$ . Additionally, the method aligns with the 6th, 7th, and 9th principles of Green Chemistry if carried out under visible or solar light, and the photocatalyst is made using renewable feedstocks.

Due to the advantages of photocatalysis in MPs degradation, researchers have made advances in addressing this issue through various photocatalytic materials. Zinc oxide nanorods degraded low-density polyethylene (LDPE) microplastic in visible light [26]. Likewise, the degradation of LDPE film in water was studied in visible-light-induced plasmonic photocatalysts comprising platinum nanoparticles deposited on zinc oxide nanorods ( $\text{ZnO-Pt}$ ) [27]. Furthermore, hydroxy-rich ultrathin  $\text{BiOCl}$  ( $\text{BiOCl-1}$ ) synthesized with mannitol was used to degrade high-density polyethylene microspheres (PE-S) [28]. Also,  $\text{M-2/Z}_{0.6}\text{C}_{0.4}\text{S}$  photocatalyst was fabricated for  $\text{H}_2$  production and simultaneously degrading polyethylene terephthalate (PET) [29].

Although several materials have been investigated for the photocatalytic degradation of microplastics, the  $\text{TiO}_2$  semiconductor has been the most extensively studied. This semiconductor has been widely studied in the scientific community with other applications due to its safety, low cost, chemical stability, efficient photoactivity and safety. Likewise, it has presented favourable results in the degradation of MPs.  $\text{Ag/TiO}_2$  has been studied for MPs and *E. coli* disinfection achieving 81% MPs degradation after 4 h in UV light [30]. Also, an optofluidic microreactor of  $\text{TiO}_2$  was tested for water purification, showing that polystyrene (PS) could be degraded with this system [31]. Photocatalytic polyacrylamide grafted  $\text{TiO}_2$  ( $\text{PAM-g-TiO}_2$ ) with LDPE nanocomposite film was irradiated for 520 h under UV light resulting in 39.85% of weight reduction and 94.60% average molecular weight ( $\text{M}_w$ ) reduction [32]. Polyethylene (PE) MPs reached a 76% mass degradation under UV irradiation for four h using a composite of  $\text{TiO}_2$  with Ag and reduced Graphene oxide [33].

Titania's photocatalytic activity depends on the semiconductor's surface and structural characteristics, including its surface area, crystal composition, particle size distribution, band gap, and other factors. Therefore, the semiconductor characteristics are essential in MPs degradation. In this work, several green  $\text{TiO}_2$ -based semiconductors were prepared using the extrapallial fluid (EPF) of *Mytilus edulis* sea water mussels as doping precursor. The semiconductors were characterized to determine their potential ability for photocatalytic purposes and then used as films or powders to photocatalytically degrade polystyrene (PS) NPs and MPs and polyethylene (PE) MPs.

## 2. Materials and Methods

### 2.1. Doping Precursors Preparation and SDS-PAGE Profiling of *Mytilus edulis* Extrapallial Fluid

The proteins contained in the extrapallial fluid (EPF) of a population of fresh blue mussels (*Mytilus edulis*) collected from Ensenada, Mexico (31.8667°N, 116.5964°W) were used as green doping precursors (i.e., a green source of carbon and nitrogen) of TiO<sub>2</sub>. The EPF was collected using the methodology previously reported by Zeng et al. [39]. The EPF was extracted gently from the mussels using a syringe and combined to produce a composite sample. The composite sample was clarified by centrifugation at 13,000 rpm for 10 min using an Eppendorf 5415D centrifuge (Eppendorf AG, Hamburg, Germany). The total protein content of the composite sample was quantified by the Bradford Method [40] using a Cary 50 UV-Vis spectrophotometer from Agilent Technologies. After protein quantification, the as-extracted EPF was labelled as C10 doping precursor. The as-extracted EPF was also submitted to a 10% sodium dodecyl sulfate-polyacrylamide gel electrophoresis (SDS-PAGE) to determine its proteins' profile (MiniProtean II, BioRad Laboratories, Inc.; Hercules, CA, United States) using a 6,500-200,000 Da protein molecular weight ladder as reference (SigmaMarker wide range; Merck KGaA; Darmstadt, Germany). Two lots were analysed. The C10 sample was used as the doping precursor with the lowest protein content. Additionally, two aqueous solutions with higher protein content were prepared through freezing (-20 °C for 12 h) and lyophilization of the as-extracted EPF. These concentrated precursor solutions with protein concentrations of 600 and 1200 ppm were labelled as C600 and C1200, respectively.

### 2.2. Synthesis and Characterization of the C-N-TiO<sub>2</sub> Semiconductors

Several C,N-TiO<sub>2</sub> semiconductors were prepared using either a hydrothermal synthesis or an hydrothermal synthesis plus calcination. These two different procedures were performed to verify if semiconductors with a higher crystallization degree derived from calcination lead to an increased photocatalytic removal of nano and microplastics from aqueous dispersions. First, the hydrothermal synthesis using titanium (IV) butoxide (97%, Sigma Aldrich) as TiO<sub>2</sub> precursor and the three doping precursors obtained in Section 2.1 was carried out using the same methodology reported by Zeng et al. [39]. Samples were labelled as M10, M600 and M1200 for the materials obtained with the C10, C600 and C1200 precursor solutions, respectively. After characterization and photocatalytic tests, sample M10 was selected to further investigation. Then, M10 semiconductor was calcined in air atmosphere at 400 °C, 600 °C and 800 °C for 3 h. These samples were identified as M10-400, M10-600 and M10-800. For the photocatalytic experiments, the M10, M600 and M1200 semiconductors were used as films deposited on clean glass substrates (using a 10 wt./v % aqueous dispersion of C,N-TiO<sub>2</sub> and a CGV USB Dip-coater with an immersion and emersion rate of 100 mm/min), while the M10, M10-400, M10-600 and M10-800 semiconductors were used as powders dispersed in an aqueous reaction medium.

Characterization of all semiconductors was performed using several analytical techniques. Crystalline phases were analysed by X-ray diffraction (XRD) in a Siemens D5000 diffractometer with Cu K $\alpha$ 1 radiation. Carbon and nitrogen doping was determined by elemental analysis by a CHNS/O Analyzer 2400 Perkin Elmer Series II instrument, at a combustion temperature of 975 °C, using a reducing column with helium at 88 °C. The bandgap ( $E_g$ ) was calculated from the diffuse reflectance spectra (DRS) of all semiconductors using the Kubelka-Munk model  $F(R) = (1-R)^2/2R$ , where  $F(R)$  is the reflectance transformed according to Kubelka-Munk theory and  $R$  is the reflectance. The  $E_g$  value was obtained by extrapolating the linear portion of a plot of  $[F(R)hv]^{1/2}$  vs  $E$  in eV to  $[F(R)hv]^{1/2} = 0$ . The reflectance spectra were collected in the 300-800 nm range on a Jasco V-670 UV-Vis/NIR spectrophotometer equipped with an ILN-725 integration sphere. The surface area was estimated by nitrogen adsorption using a Micromeritics TriStar II Plus 3.01 surface area analyser (analysis bath temperature of 77.3 K, equilibration interval of 5 s, and degasification at 110 °C). Microstructural observation was carried out by Field Emission Gun Scanning Electron Microscopy (FEG-SEM), using a FEI Nova NanoSEM 450 Field Emission SEM.

### 2.3. MPs and NPs Obtainment and Characterization

Primary PS MPs and NPs were prepared by the surfactant-free emulsion polymerization synthesis reported by Telford et al. [41]. The reaction was conducted for 10 min or 20 h to obtain PS NPs or MPs, respectively. Primary PE MPs were obtained from a commercial facial scrub using the extraction methodology proposed by Napper et al. [42]. Polymer type was confirmed by ATR-FTIR. The particle size and morphology of all MPs and NPs was evaluated by optical microscopy (OM) using a Leica DME microscope with a Leica ICC50 W camera or by SEM, using a Thermo-Fisher Scientific FEI Quanta 200 E-SEM (environmental SEM). Microchemical analysis was also conducted by energy dispersive X-ray spectroscopy (EDS) using an Oxford INCA-350 system coupled to the SEM microscope. Before the analysis, the samples were coated with a gold layer of 10 nm.

### 2.4. Photocatalytic Experiments

#### 2.4.1. Photocatalysis of Primary PS NPs and MPs

50 mL of a 2 wt./vol % aqueous dispersion of the PS NPs or 50 mL of a 0.01 wt./vol % aqueous dispersion of the PS MPs were placed in a batch-type glass reactor of 100 mL capacity. The M10, M600 or M1200 films were then immersed in the dispersion, ensuring that the dispersion covered all surface of the semiconductor's film. The reactor was then transferred inside a photocatalytic reaction chamber equipped with a constant temperature bath ( $\pm 2$  °C) and an ARTlite Slim LED IP65 50W (ARE-006 model) visible LED lamp (400 – 800 nm) placed at 25 cm from the sample ( $57.2 \pm 0.3$  W/m<sup>2</sup>). Agitation was set at 300 rpm. Adsorption of PS on the semiconductors' surface was conducted in the darkness for 1 h. After adsorption process, the lamp was turned on and photocatalysis was conducted for 5 h at T<sub>room</sub>. Photolysis tests were also carried out at the same conditions, but using a C<sub>x</sub>N-TiO<sub>2</sub>-free glass substrate. PS degradation was followed by turbidimetry, using a Lovibond TB 250 WL turbidimeter and a calibration curve that related NTU units with PS NPs or MPs concentration [25,43]. Two replicates were performed for all the photocatalytic experiments, and the mean  $\pm$  S.D. values are reported.

#### 2.4.2. Photocatalysis of Primary PE MPs

The photocatalytic experiments' reaction conditions were carried out according to our previous work, which demonstrated the photocatalytic degradation of HDPE MPs using a C<sub>x</sub>N-TiO<sub>2</sub> material [34]. Therefore, photocatalysis was conducted in a Batch-type glass reactor, using 50 mL of a 0.4 wt./vol % PE MPs dispersion (pH 3) and a semiconductor load of 200 mg. The reactor was placed in the photocatalytic reaction chamber with the temperature set at  $0 \pm 2$  °C. PE MPs were dispersed in the experiments by continuous stirring at 350 rpm. Adsorption of the powdered semiconductors on the PE's surface was conducted in the darkness for 2 h. Afterwards, photocatalysis was carried out for 50 h. After photocatalysis, the residual (degraded) PE MPs were separated from the reaction system and washed twice with distilled water to remove potential C<sub>x</sub>N-TiO<sub>2</sub> traces that could remain attached. Two replicates were performed for all the photocatalytic experiments, and for the mean  $\pm$  S.D. values are reported. PE MPs degradation was followed by gravimetry, FTIR and microscopy. Gravimetry was used to follow degradation because it represents a simple and direct way to quantify the polymers' degradation [44]. Mass measurements were performed in an ACZET CY224C analytical balance.

## 3. Results and Discussion

### 3.1. Protein Quantification of *M. edulis* EPF

The protein content in the clarified composite EPF of *M. edulis* (as-extracted EPF) was reported as  $9.93 \pm 0.05$  ppm.

### 3.2. Semiconductors Characterization

Figure 1a displays the XRD patterns of all the semiconductors prepared here, showing that they are all composed of anatase  $\text{TiO}_2$  (JCPDS file No. 00-021-1272), except M10 sample, which also presents two small peaks at 36 and 44° that are characteristic of rutile  $\text{TiO}_2$  (JCPDS file No. 01-076-0317). Interestingly, it was found that when protein concentration was increase from  $9.93 \pm 0.05$  ppm (M10 sample) to 600 ppm or 1200 ppm, rutile peaks disappear and only anatase was present in the XRD patterns of the M600 and M1200 semiconductors. This result is in well agreement with that reported by Zeng et al. [39], whom first proposed using the same hydrothermal procedure but with the EPF of *Cristaria plicata* fresh water mussels to synthetize hierarchically porous N- $\text{TiO}_2$ . In their investigation, authors found that the EPF proteins controls the crystalline phase of the semiconductor, and significantly prevents the formation of other  $\text{TiO}_2$  polymorphs [39]. Thermal stability of anatase phase in semiconductors designed for photocatalytic purposes is a key factor for their performance. This is because anatase is often preferred to rutile and brookite  $\text{TiO}_2$  polymorphs due to its higher photocatalytic efficiency [45]. Anatase to rutile transformation usually occurs at 500 – 700 °C [46]. Here, the blue, purple and orange XRD patterns of Figure 1a shows that even if the M10 sample was thermally treated at the temperature interval that promotes rutile formation (400 – 800 °C), the presence of the EPF from sea water mussels avoid formation of such  $\text{TiO}_2$  polymorph, increasing the thermal stability of anatase phase in the prepared semiconductors. As expected, Figure 1a also shows that calcination after hydrothermal treatment led to more crystalline semiconductors compared to those prepared using only hydrothermal synthesis, being the M10-800 sample the most crystalline one.

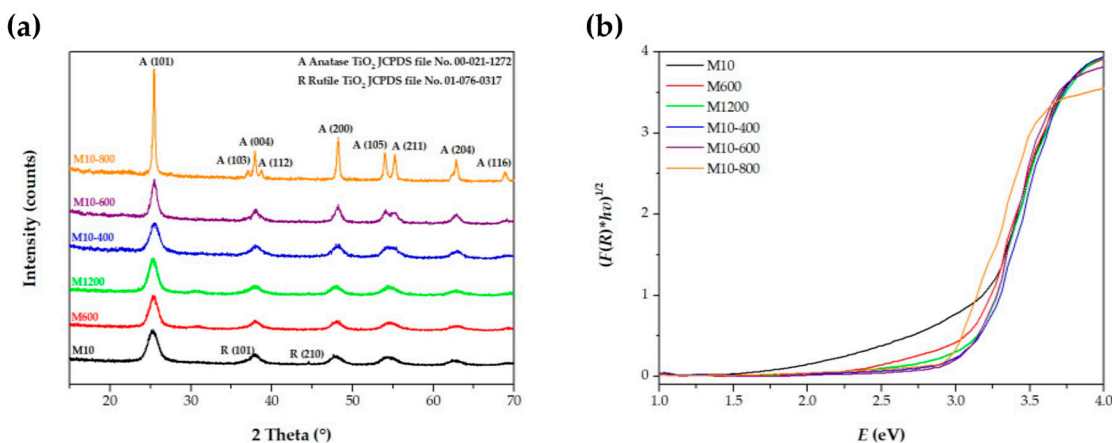


**Figure 1.** (a) XRD patterns and (b)  $[F(R)hv]^{1/2}$  vs  $E$  plots.

**Table 1.** Properties of the semiconductors.

Semiconductor	$E_g$ (eV)	Wavelength of Light Absorption (nm)	Carbon (wt.%)	Nitrogen (wt.%)	$S_{\text{BET}}$ ( $\text{m}^2/\text{g}$ )
M10	2.93	423	1.37	0.41	223.2
M1600	2.87	432	0.29	0.16	171.15
M1200	2.95	421	0.28	0.20	192.8
M10-400	2.88	431	4.44	0.42	166.48
M10-600	3.02	411	4.58	0.32	76.73
M10-800	2.99	415	10.37	0.34	6.04

Figure 1b presents the  $[F(R)hv]^{1/2}$  vs  $E$  plots calculated from the diffuse reflectance spectra of the different semiconductors. For an easy reading of the obtained  $E_g$  values, these are also enlisted in Table 1. It was found that the presence of the doping precursors derived from the *M. edulis* EPF promote a reduction of the bandgap of  $\text{TiO}_2$  from its standard value of 3.20 [47] eV to 2.93, 2.87 and

2.95 eV for the M10, m600 and M1200 semiconductors, respectively, allowing them the absorption of visible light as shown in Table 1. Moreover, it was found that after calcination, the M10 sample's ability of absorbing visible light is not lost. As shown in Figure 1b and Table 1, the M10 calcined samples present  $E_g$  values lower than 3.1 eV, which is the lowest threshold for a semiconductor to present activity in the visible portion of the electromagnetic spectrum. The doping elements responsible of these low  $E_g$  values were determined by elemental analysis. Table 1 shows that all the semiconductors prepared here contain nitrogen and carbon in different amounts. In a previous report, it was demonstrated that no one of these elements was found for an undoped  $\text{TiO}_2$  prepared by the same hydrothermal procedure but using distilled water instead the EPF [34], demonstrating that carbon and nitrogen dopants are derived from the proteins of the EPF of the *M. edulis* mussels. Indeed, when analysed on SDS-PAGE, the EPF exhibited mixed molecular weight proteins, ranging from around 10 up to 200 kDa (Figure 2). This wide variety of proteins can be regarded as a mixture of different sized macromolecules that could interact differently with  $\text{TiO}_2$  during the synthesis of the semiconductor through both C- or N- terminal moieties. When the material is subjected to heat treatment (hydrothermal synthesis or calcination), the proteins tend to degrade by thermal decomposition. However, some carbon and nitrogen seem to remain on the  $\text{TiO}_2$  network, promoting a modification of the  $E_g$  value and photocatalytic activity in visible light.

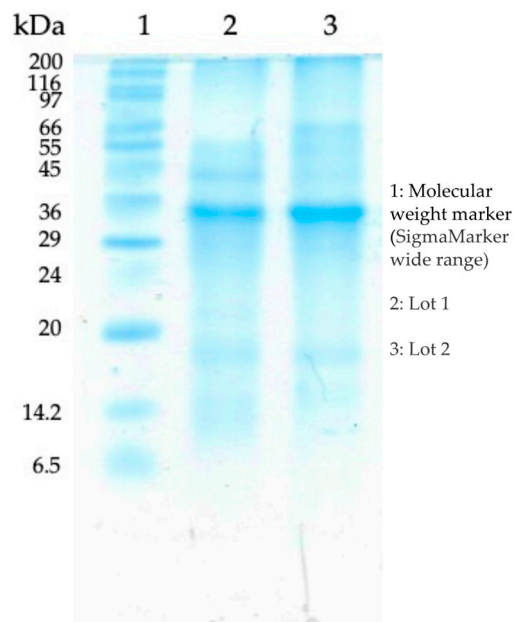


**Figure 2.** SDS-PAGE profiling of *Mytilus edulis* extrapallial fluid.

As shown in Table 1, increasing the protein concentration from  $9.93 \pm 0.05$  ppm (M10 sample) to 600 ppm or 1200 ppm (M600 and M1200 samples) decreases both carbon and nitrogen content in the  $\text{TiO}_2$  semiconductors. This result was not expected, as it was thought that increasing the protein concentration should raise the availability of C- or N- terminal moieties for interaction with  $\text{TiO}_2$ . Then, it seems likely that some components of the as-extracted EPF that were present in the composite liquid (additional to proteins) were not removed in the clarification process and act as additional sources of carbon and nitrogen during the synthesis process. The absence of those components in the 600 ppm and 1200 ppm protein aqueous solutions can explain their lower carbon and nitrogen content. This hypothesis will be the object of a future investigation.

Furthermore, Table 1 shows that calcination of M10 samples did not negatively influence the doping content of the semiconductor samples. In the case of nitrogen doping, a slight drop in its concentration was observed. On the other hand, carbon content raised when increasing calcination temperature. This can be related to the carbonization of organic residues from the synthesis (butoxide residues or EPF components) during calcination at higher temperatures.

Figure 3 displays the FEG-SEM micrographs at different magnifications of the C<sub>x</sub>N-TiO<sub>2</sub> semiconductors prepared at different protein concentrations. For all three samples, at low magnification values (10,000x and 40,000x), the micrographs show that the semiconductors are composed of particles of 1-10  $\mu$ m of diameter. At high magnification (400,000X), it can be observed that these large particles are in turn formed by small particles of approximately 10 nm of diameter (Figures 3c,f,i). In all samples, some degree of porosity derived from the agglomeration of particles is observed (Figures 3b,e,g). In sample M1200, a partial sinterization of the particles can be observed (Figure 3h). This particular microstructure was related to both the high protein content of the aqueous solution used to prepare this semiconductor (1200 ppm) and the characteristics of the EPF. The presence of a prominent protein at 35 kDa in the SDS-PAGE profiling of Figure 2 could be related to the fact that, despite having a wide variety of proteins, the EPF produces relatively homogeneous pore sizes along the surface of the mesoporous semiconductor CN-TiO<sub>2</sub> after heat treatment.

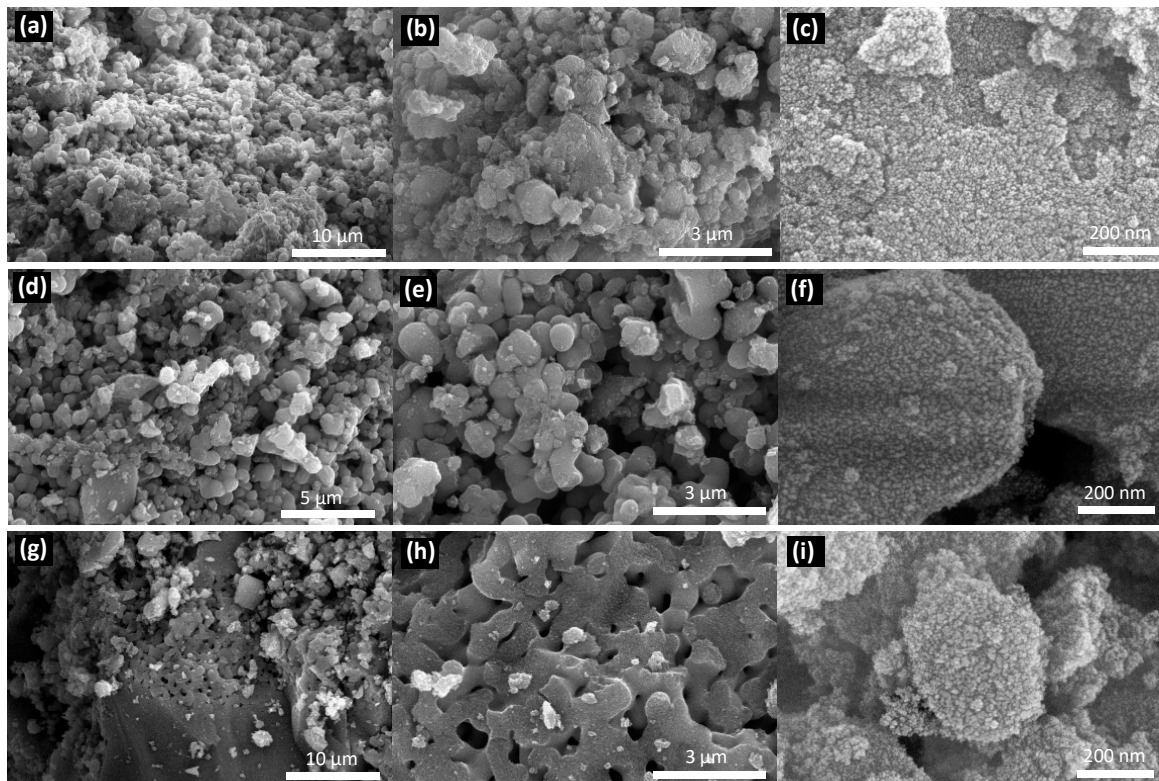


**Figure 3.** FEG-SEM micrographs of the C<sub>x</sub>N-TiO<sub>2</sub> semiconductors prepared at different protein concentrations. (a) M10 10,000x; (b) M10 40,000x; (c) M10 400,000x; (d) M600 10,000x; (e) M600 40,000x; (f) M600 400,000x; (g) M1200 10,000x; (h) M1200 40,000x and (i) M1200 400,000x.

The characteristic morphology of samples M10, M600 and M1200 shown in Figure 3 lead to a high surface area. As shown in Table 1, surface areas are between 223 and 192 m<sup>2</sup>/g. These values are 3.86-4.46 times bigger than the surface area of commercial TiO<sub>2</sub> (Aeroxide® P25, 50 m<sup>2</sup>/g [48]) and 1.53-1.77 times higher than the best photocatalysis obtained by Zeng et al. using the same procedure but with the EPF derived from *C. plicata* mussels. Table 1 also shows that calcination leads to a decrease of the surface area of M10 sample, which is more drastic at the highest calcination temperature (800 °C). This result was expected, as calcination usually led to sinterization and densification of the samples. These phenomena usually promote closing of porosity and growing of the particles, both process that induce a reduction of the surface area of the semiconductors. The changes in the microstructure of the calcined samples are presented in the Figure 4, which displays the FEG-SEM micrographs of the M10 semiconductor calcined at 400, 600 and 800 °C. Growing of the particles can be easily observed at low magnification (10,000x) while densification at higher

magnifications (100,000x and 200,000x). The drastic loss of surface area in sample M10-800 was also related to the formation of 10  $\mu\text{m}$  dense particles (Figure 4g).

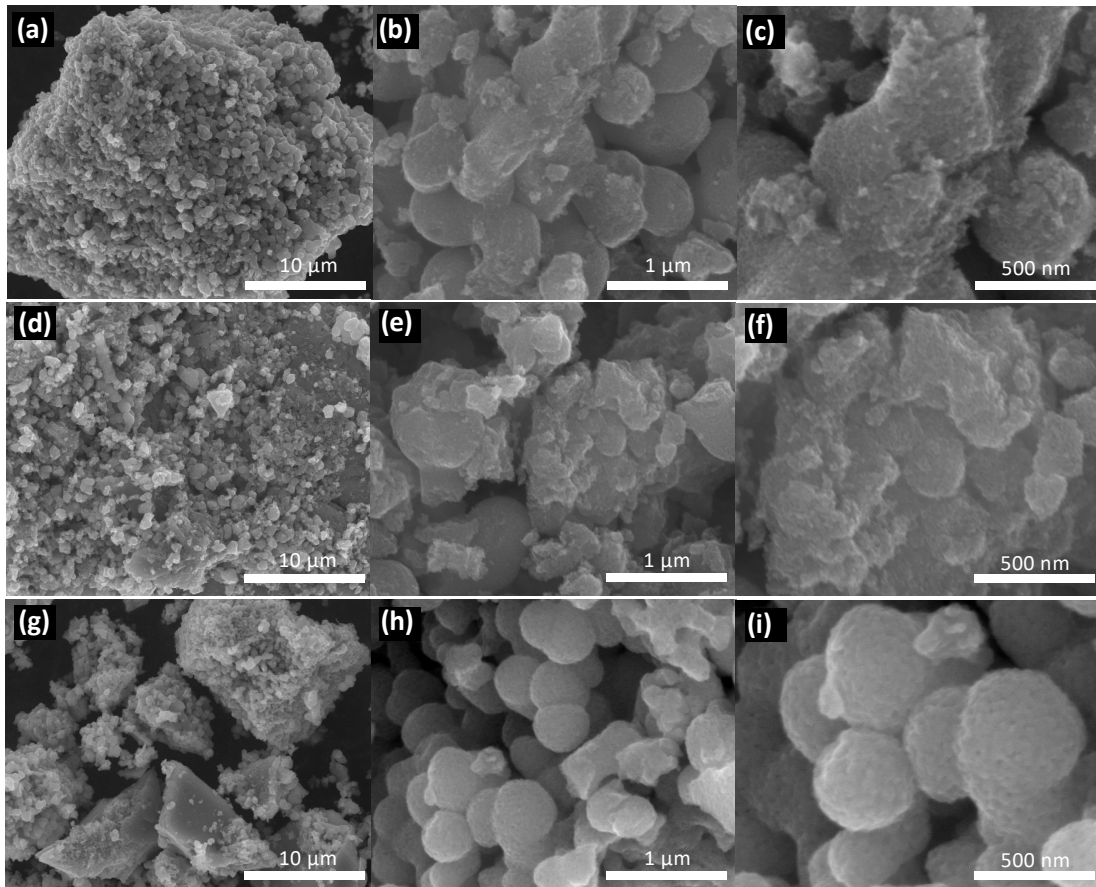


**Figure 4.** FEG-SEM micrographs of the M10 C,N-TiO<sub>2</sub> calcined at 400, 600 and 800 °C. (a) M10-400 10,000x; (b) M10-400 100,000x; (c) M10-400 200,000x; (d) M10-600 10,000x; (e) M10-600 100,000x; (f) M10-600 200,000x; (g) M10-800 10,000x; (h) M10-800 100,000x and (i) M10-800 200,000x.

### 3.3. PS NPs and MPs Characterization

Figure 5 shows the SEM micrographs of the prepared PS NPs and MPs, respectively. PS MPs present sizes of  $1.04 \pm 0.03 \mu\text{m}$  while PS NPs have sizes of  $278.6 \pm 9.1 \text{ nm}$ . The inset in Figure 5a shows that both materials are composed of PS, as its characteristic absorption bands are present in both FTIR spectra. These results confirmed that the PS particles synthesized can be considered primary PS NPs and MPs and be further used for conducting the photocatalytic experiments.

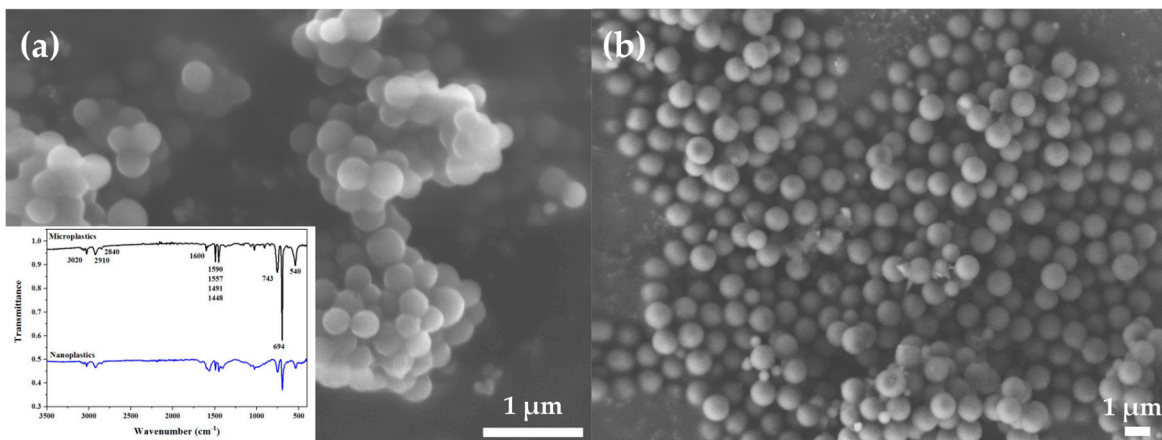


**Figure 5.** SEM micrographs of the PS (a) NPs (20,000x) and (b) MPs (5,000x). Inset in (a): FTIR spectra of the PS NPs and MPs.

### 3.4. Photocatalysis of Primary PS NPs and MPs Using $C_xN-TiO_2$ Films

The photocatalytic removal of PS NPs and MPs from aqueous dispersions was conducted for 5 hours of visible light irradiation. This reaction time was selected because increases in the reaction time did not promote further reductions in the concentration of PS, demonstrating that high degradation efficiencies for the photocatalytic removal of PS NPs and MPs are hard to achieve [25,43]. Adsorption experiments did not promote changes in PS concentration, indicating that the polymer was not adsorbed on the films. The null adsorption of PS on the surface of the films was attributed to the high pH value of the PS dispersions (11-12 due to the NaOH residues from the synthesis procedure [41]) that weaken the electrostatic interactions between the oxide surface and the PS [25,43]. As displayed in Figure 6, for both sizes, photolysis resulted in a limited reduction of the concentration of PS polymer. Degradation of PS plastics in visible light has been previously reported [25,49]. On the other hand, the presence of the different  $C_xN-TiO_2$  films in the reaction media promoted a greater removal of PS NPs and MPs. This reduction was attributed to the formation of several chemical species ( $h^+$ ,  $e^-$  and reactive oxygen species (ROS)) in the surface of the semiconductors and their interaction with the PS particles, as previously demonstrated [50]. Comparing the three prepared samples, it was found that the M10 sample present the best performance (although only slight differences in the efficiency removal between the samples were detected).

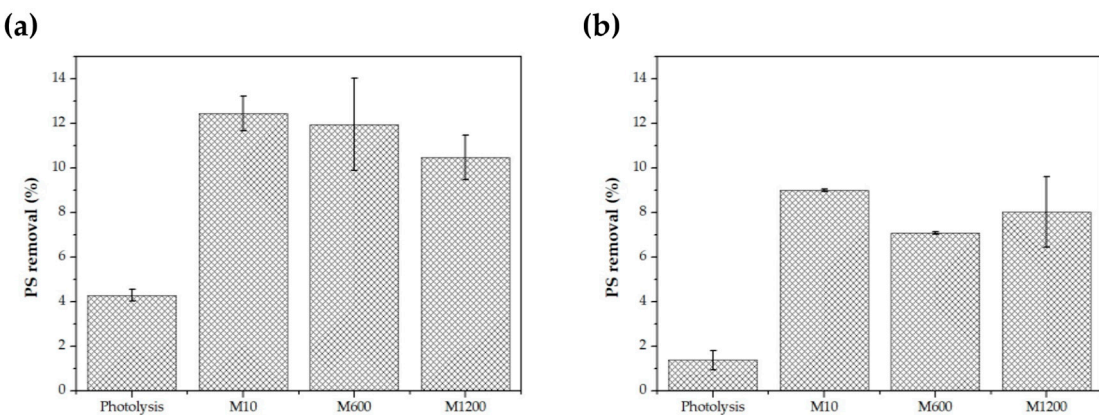


**Figure 6.** Photocatalysis of PS (a) NPs and (b) MPs using the M10, M600 and M1200 semiconductors in the form of films. Photolysis is also shown.

The limited removal efficiency (maximum 12.45%) of PS was related to the intrinsic disadvantages associated to the use of the semiconductors in the form of films for MPs photocatalysis purposes. In one hand, for these experiments, the semiconductors were used as films because they avoid problems with the reuse of the semiconductor, as powders are usually difficult to separate from the reaction medium after photocatalysis. Using semiconductor as films and not as powders can be a great advantage if this technology is intended to be applied as tertiary treatment in WWTPs. However, when using films, part of the high surface area of the synthesized powders is lost when depositing them over the glass substrates. Additionally, adsorption of the semiconductor in the PS particles (either NPs or MPs) is not allowed, limiting the interaction between the pollutant and the chemical species generated at the surface of the semiconductor. As stated in our previous report, the interaction of MPs and semiconductors in the form of powders can help to increase degradation efficiency [34].

Due to the previous motivations, photocatalysis of MPs using the semiconductor in the form of powders was also tested. As separation of PS after reaction is difficult due to the small size of the NPs and MPs, bigger PE microplastics were used to conduct the experiments. Also, as M10 sample

presented the best characteristics for photocatalytic purposes (section 3.2) and its synthesis requires less effort and energetic cost compared to the synthesis of the M600 and M1200 samples, the M10 C<sub>x</sub>N-TiO<sub>2</sub> semiconductor was selected to conduct the photocatalysis of PE MPs. Finally, comparisons between the original M10 sample and the same sample calcined at different temperatures was performed to determine if higher crystallization degree has an influence on the degradation efficiency.

### 3.5. PE MPs Characterization

Figure 7a displays the FTIR analysis carried out on the microbeads extracted from the facial scrub. The characteristic vibrational bands of high-density polyethylene at 2911 and 2846 cm<sup>-1</sup> that correspond to the asymmetric and symmetric stretching vibrations of the CH<sub>2</sub> group and the bands at 1463 and 719 cm<sup>-1</sup> that correspond to the scissoring and rocking bending vibrations of the same group were identified [51]. Figure 7b displays an optical micrograph (8x) of the same microbeads. It was found that they have an average size of 725 ± 108 µm. The surface of the microbeads was further investigated by SEM (Figures 7c,d). SEM micrographs revealed that the surface of the microbeads exhibited a homogeneous roughness, which may be related to their application as abrasive in facial scrubs. These results confirmed that the blue microbeads extracted from the commercial facial scrub can be considered primary MPs of PE and be further used for conducting photocatalytic experiments.

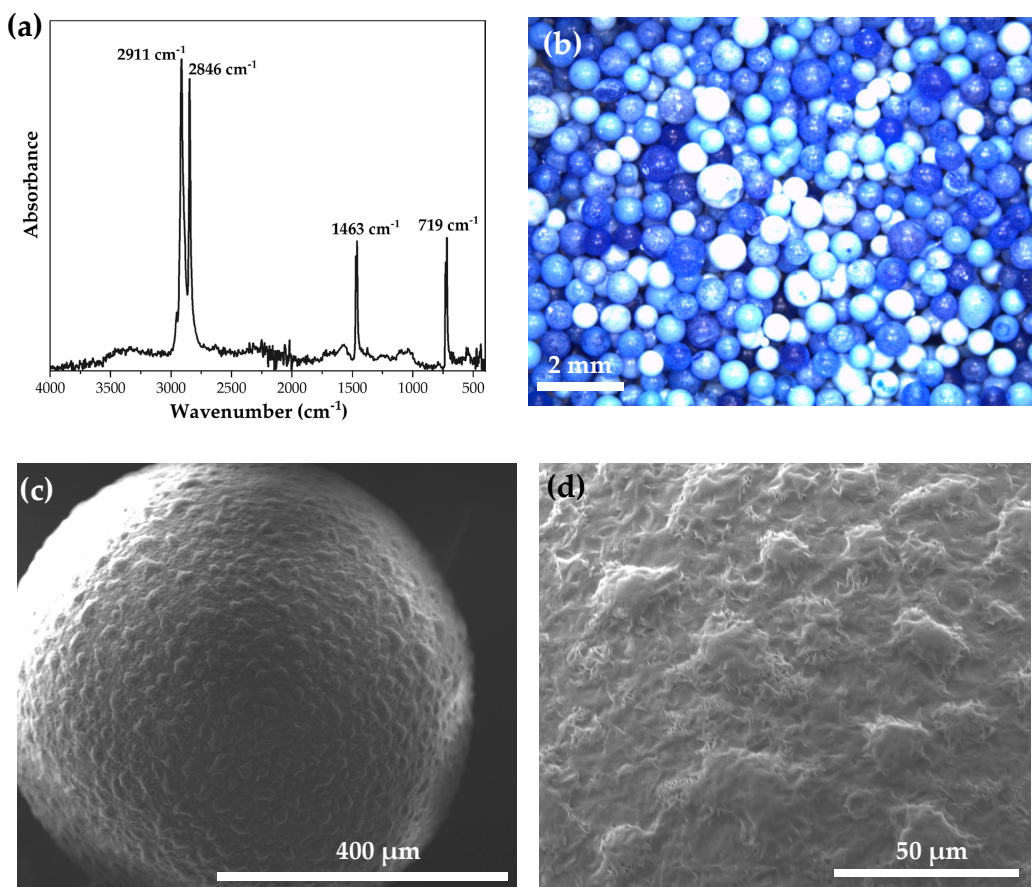


**Figure 7.** (a) FTIR spectrum; (b) Optical micrograph (8x) and (c,d) SEM micrographs (400x and 2000X, respectively) of the PE MPs.

### 3.6. Photocatalysis of Primary PE MPs Using C,N-TiO<sub>2</sub> Powders

Figure 8 shows that photolysis of PE MPs did not promote changes in the MPs concentration, indicating that the experimental conditions do not promote degradation. As previously reported, the photocatalysis of PE MPs using the powdered M10 C,N-TiO<sub>2</sub> at low temperature (0 °C) and pH value (3) reached a mass loss of  $71.77 \pm 1.88\%$  [34]. Cold temperature promotes the fragmentation of the original PE MPs into smaller particles. This size reduction allowed a better interaction between the plastic and the C,N-TiO<sub>2</sub> powders. On the other side, pH increases the concentration of H<sup>+</sup> ions in the reaction media, favouring the photodegradation mechanism generally proposed for PE plastic [34]. As observed in Figure 8, calcination has an influence in the degradation of PE MPs, and this influence depends on the temperature. At relatively low temperatures (400 °C and 600 °C), mass loss after photocatalysis decreases, even if such semiconductors have characteristics that makes them good candidates for photocatalytic purposes such as anatase crystalline phase, activity in visible light and high surface area (see Figure 1 and Table 1). Therefore, the decrease in the degradation efficiency when performing photocatalysis with those samples was related to their densification and decrease of surface area. However, the results displayed in Figure 8 show that the higher crystallinity of M800 (calcined at 800 °C) sample can be key factor for increasing degradation efficiency. This result is interesting because on M400 and M600 samples densification of the C,N-TiO<sub>2</sub> particles was not as pronounced as in the M10-800 sample, and this latter still shown the best performance. It has been reported that for improving the photocatalytic performance of anatase TiO<sub>2</sub>, it is necessary to simultaneously increase its crystallinity and surface area [52]. However, this affirmation should be analyzed in relation to the characteristics of the model pollutant to degrade, because frequently, it is a chemical specie that can easily adsorb on the surface of the anatase semiconductor. Since the "big" MPs PE used here can have a particle size that are up to 72 times bigger than the size of the semiconductor's particle, it has to be considered that MPs cannot be adsorbed on its surface, and then surface area of the semiconductor, although important, may have a minor role in influencing the photocatalytic degradation efficiency of MPs. The results shown in Figure 8 suggest that crystallinity can be a more determinant factor to take into account when performing photocatalysis of MPs.

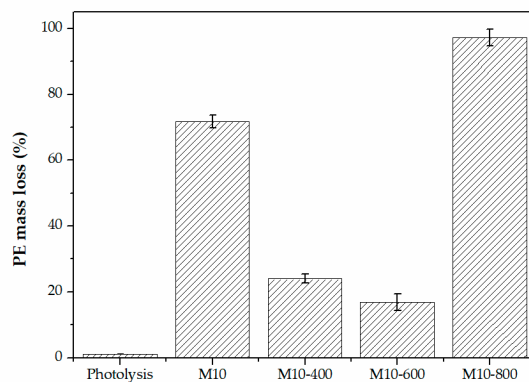


**Figure 8.** Photocatalysis of PE MPs using the M10, M10-400, M10-600 and M10-800 semiconductors (as powders). Photolysis is also shown.

## 4. Conclusions

MPs and NPs are complex aquatic pollutants that can be degraded by photocatalysis. In this work, it was found that the properties of the photocatalyst should be carefully designed in order to achieve degradation efficiency that allow the application of this technology to reduce marine MPs pollution. The obtention of green TiO<sub>2</sub>-based semiconductors with characteristics that makes them good candidates for photocatalytic purposes (such as anatase crystalline phase, presence of porosity, activity in visible light and high surface area) seems not enough to achieve high degradation

efficiency. The operational conditions of the reaction system should be also taken into account. For instance, the convenience of using semiconductors in the form of films for photocatalytic degradation of MPs can be overcome by their limited surface area or the null adsorption of the semiconductor in the MPs particles. Additionally, when it was found that that crystallinity of the semiconductor can be a more determinant factor to take into account when performing photocatalysis of MPs using powdered semiconductors.

**Author Contributions:** Conceptualization, E.I.C.G.; Funding acquisition, E.I.C.G.; Investigation, A.D.V.G., M.C.A.T. I.S. and C.A.R.G.; Methodology, E.I.C.G., A.D.V.G., C.A.R.G., I.S. and M.C.A.T.; Supervision, E.I.C.G., J.F.V.C.; Project administration, E.I.C.G.; Resources, E.I.C.G. and J.F.V.C.; Writing—original draft preparation, A.D.V.G. and E.I.C.G.; Writing—review and editing, E.I.C.G., M.C.A.T. and J.F.V.C. All authors have read and agreed to the published version of the manuscript. All authors have read and agreed to the published version of the manuscript.

**Funding:** This research was funded by Consejo Nacional de Ciencia y Tecnología (Mexico), grant number APN-2017/5167 and by Secretaría de Educación Pública (Mexico), Grant number 511-6/18-8928.

**Institutional Review Board Statement:** “Not applicable”.

**Data Availability Statement:** The data that supports the findings of this study are available from the corresponding author, [E.I.C.G.], upon reasonable request.

**Conflicts of Interest:** The authors declare no conflict of interest.

## References

1. Ritchie, H.; Roser, M. Plastic Pollution. *Our World in Data* **2018**.
2. Gall, S.C.; Thompson, R.C. The Impact of Debris on Marine Life. *Marine Pollution Bulletin* **2015**, *92*, 170–179, doi:10.1016/j.marpolbul.2014.12.041.
3. Law, K.L. Plastics in the Marine Environment. *Annual Review of Marine Science* **2017**, *9*, 205–229, doi:10.1146/annurev-marine-010816-060409.
4. Committee for Risk Assessment (RAC); Committee for Socio-economic Analysis (SEAC) *Background Document to the Opinion on the Annex XV Report Proposing Restrictions on Intentionally Added Microplastics*; European Chemicals Agency (ECHA): Helsinki, Finland, 2000;
5. Pizzurro, F.; Recchi, S.; Nerone, E.; Salini, R.; Barile, N.B. Accumulation Evaluation of Potential Microplastic Particles in *Mytilus Galloprovincialis* from the Goro Sacca (Adriatic Sea, Italy). *Microplastics* **2022**, *1*, 303–318, doi:10.3390/microplastics1020022.
6. Prata, J.C.; Silva, A.L.P.; da Costa, J.P.; Dias-Pereira, P.; Carvalho, A.; Fernandes, A.J.S.; da Costa, F.M.; Duarte, A.C.; Rocha-Santos, T. Microplastics in Internal Tissues of Companion Animals from Urban Environments. *Animals* **2022**, *12*, 1979, doi:10.3390/ani12151979.
7. Yang, D.; Shi, H.; Li, L.; Li, J.; Jabeen, K.; Kolandhasamy, P. Microplastic Pollution in Table Salts from China. *Environ. Sci. Technol.* **2015**, *49*, 13622–13627, doi:10.1021/acs.est.5b03163.
8. Schymanski, D.; Goldbeck, C.; Humpf, H.-U.; Fürst, P. Analysis of Microplastics in Water by Micro-Raman Spectroscopy: Release of Plastic Particles from Different Packaging into Mineral Water. *Water Research* **2018**, *129*, 154–162, doi:10.1016/j.watres.2017.11.011.
9. Kutralam-Muniasamy, G.; Pérez-Guevara, F.; Elizalde-Martínez, I.; Shruti, V.C. Branded Milks – Are They Immune from Microplastics Contamination? *Science of The Total Environment* **2020**, *714*, 136823, doi:10.1016/j.scitotenv.2020.136823.
10. Rochman, C.M.; Tahir, A.; Williams, S.L.; Baxa, D.V.; Lam, R.; Miller, J.T.; Teh, F.-C.; Werorilangi, S.; Teh, S.J. Anthropogenic Debris in Seafood: Plastic Debris and Fibers from Textiles in Fish and Bivalves Sold for Human Consumption. *Sci Rep* **2015**, *5*, 14340, doi:10.1038/srep14340.
11. Leslie, H.A.; van Velzen, M.J.M.; Brandsma, S.H.; Vethaak, A.D.; Garcia-Vallejo, J.J.; Lamoree, M.H. Discovery and Quantification of Plastic Particle Pollution in Human Blood. *Environment International* **2022**, *163*, 107199, doi:10.1016/j.envint.2022.107199.
12. Ragusa, A.; Svelato, A.; Santacroce, C.; Catalano, P.; Notarstefano, V.; Carnevali, O.; Papa, F.; Rongioletti, M.C.A.; Baiocco, F.; Draghi, S.; et al. Plasticenta: First Evidence of Microplastics in Human Placenta. *Environment International* **2021**, *146*, 106274, doi:10.1016/j.envint.2020.106274.
13. Schwabl, P.; Köppel, S.; Königshofer, P.; Bucsics, T.; Trauner, M.; Reiberger, T.; Liebmann, B. Detection of Various Microplastics in Human Stool: A Prospective Case Series. *Annals of Internal Medicine* **2019**, *171*, 453–457, doi:https://doi.org/10.7326/M19-0618.
14. Rodrigues, J.P.; Duarte, A.C.; Santos-Echeandía, J.; Rocha-Santos, T. Significance of Interactions between Microplastics and POPs in the Marine Environment: A Critical Overview. *TrAC Trends in Analytical Chemistry* **2019**, *111*, 252–260, doi:10.1016/j.trac.2018.11.038.

15. Barus, B.S.; Chen, K.; Cai, M.; Li, R.; Chen, H.; Li, C.; Wang, J.; Cheng, S.-Y. Heavy Metal Adsorption and Release on Polystyrene Particles at Various Salinities. *Frontiers in Marine Science* **2021**, *8*.
16. Liao, Y.; Yang, J. Microplastic Serves as a Potential Vector for Cr in an In-Vitro Human Digestive Model. *Science of The Total Environment* **2020**, *703*, 134805, doi:10.1016/j.scitotenv.2019.134805.
17. López-Vázquez, J.; Rodil, R.; Trujillo-Rodríguez, M.J.; Quintana, J.B.; Cela, R.; Miró, M. Mimicking Human Ingestion of Microplastics: Oral Bioaccessibility Tests of Bisphenol A and Phthalate Esters under Fed and Fasted States. *Science of The Total Environment* **2022**, *826*, 154027, doi:10.1016/j.scitotenv.2022.154027.
18. Hamidian, A.H.; Ozumchelouei, E.J.; Feizi, F.; Wu, C.; Zhang, Y.; Yang, M. A Review on the Characteristics of Microplastics in Wastewater Treatment Plants: A Source for Toxic Chemicals. *Journal of Cleaner Production* **2021**, *295*, 126480, doi:10.1016/j.jclepro.2021.126480.
19. Ahmed, R.; Hamid, A.K.; Krebsbach, S.A.; He, J.; Wang, D. Critical Review of Microplastics Removal from the Environment. *Chemosphere* **2022**, *293*, 133557, doi:10.1016/j.chemosphere.2022.133557.
20. Ricardo, I.A.; Alberto, E.A.; Silva Júnior, A.H.; Macuvele, D.L.P.; Padoin, N.; Soares, C.; Gracher Riella, H.; Starling, M.C.V.M.; Trovó, A.G. A Critical Review on Microplastics, Interaction with Organic and Inorganic Pollutants, Impacts and Effectiveness of Advanced Oxidation Processes Applied for Their Removal from Aqueous Matrices. *Chemical Engineering Journal* **2021**, *424*, 130282, doi:10.1016/j.cej.2021.130282.
21. Lin, J.; Yan, D.; Fu, J.; Chen, Y.; Ou, H. Ultraviolet-C and Vacuum Ultraviolet Inducing Surface Degradation of Microplastics. *Water Research* **2020**, *186*, 116360, doi:10.1016/j.watres.2020.116360.
22. Zafar, R.; Park, S.Y.; Kim, C.G. Surface Modification of Polyethylene Microplastic Particles during the Aqueous-Phase Ozonation Process. *Environmental Engineering Research* **2021**, *26*, doi:10.4491/eer.2020.412.
23. Miao, F.; Liu, Y.; Gao, M.; Yu, X.; Xiao, P.; Wang, M.; Wang, S.; Wang, X. Degradation of Polyvinyl Chloride Microplastics via an Electro-Fenton-like System with a TiO<sub>2</sub>/Graphite Cathode. *Journal of Hazardous Materials* **2020**, *399*, 123023, doi:10.1016/j.jhazmat.2020.123023.
24. Kang, J.; Zhou, L.; Duan, X.; Sun, H.; Ao, Z.; Wang, S. Degradation of Cosmetic Microplastics via Functionalized Carbon Nanosprings. *Matter* **2019**, *1*, 745–758, doi:10.1016/j.matt.2019.06.004.
25. Acuña-Bedoya, J.D.; Luévano-Hipólito, E.; Cedillo-González, E.I.; Domínguez-Jaimes, L.P.; Hurtado, A.M.; Hernández-López, J.M. Boosting Visible-Light Photocatalytic Degradation of Polystyrene Nanoplastics with Immobilized CuxO Obtained by Anodization. *Journal of Environmental Chemical Engineering* **2021**, *9*, 106208, doi:10.1016/j.jece.2021.106208.
26. Tofa, T.S.; Kunjali, K.L.; Paul, S.; Dutta, J. Visible Light Photocatalytic Degradation of Microplastic Residues with Zinc Oxide Nanorods. *Environ Chem Lett* **2019**, *17*, 1341–1346, doi:10.1007/s10311-019-00859-z.
27. Tofa, T.S.; Ye, F.; Kunjali, K.L.; Dutta, J. Enhanced Visible Light Photodegradation of Microplastic Fragments with Plasmonic Platinum/Zinc Oxide Nanorod Photocatalysts. *Catalysts* **2019**, *9*, 819, doi:10.3390/catal9100819.
28. Jiang, R.; Lu, G.; Yan, Z.; Liu, J.; Wu, D.; Wang, Y. Microplastic Degradation by Hydroxy-Rich Bismuth Oxychloride. *Journal of Hazardous Materials* **2021**, *405*, 124247, doi:10.1016/j.jhazmat.2020.124247.
29. Cao, B.; Wan, S.; Wang, Y.; Guo, H.; Ou, M.; Zhong, Q. Highly-Efficient Visible-Light-Driven Photocatalytic H<sub>2</sub> Evolution Integrated with Microplastic Degradation over MXene/ZnxCd1-XS Photocatalyst. *Journal of Colloid and Interface Science* **2022**, *605*, 311–319, doi:10.1016/j.jcis.2021.07.113.
30. Haris, M.F.; Dudit, A.M.; Ibadurrohman, M.; Setiadi, S.; Slamet, S. Doped TiO<sub>2</sub> Photocatalyst for Disinfection of E. Coli and Microplastic Pollutant Degradation in Water. *Asian Journal of Chemistry* **2021**, *33*, 2038–2042, doi:https://doi.org/10.14233/ajchem.2021.23255.
31. Kim, H.; Kwon, H.; Song, R.; Shin, S.; Ham, S.-Y.; Park, H.-D.; Lee, J.; Fischer, P.; Bodenschatz, E. Hierarchical Optofluidic Microreactor for Water Purification Using an Array of TiO<sub>2</sub> Nanostructures. *npj Clean Water* **2022**, *5*, 1–10, doi:10.1038/s41545-022-00204-y.
32. Liang, W.; Luo, Y.; Song, S.; Dong, X.; Yu, X. High Photocatalytic Degradation Activity of Polyethylene Containing Polyacrylamide Grafted TiO<sub>2</sub>. *Polymer Degradation and Stability* **2013**, *98*, 1754–1761, doi:10.1016/j.polymdegradstab.2013.05.027.
33. Fadli, M.H.; Ibadurrohman, M.; Slamet, S. Microplastic Pollutant Degradation in Water Using Modified TiO<sub>2</sub> Photocatalyst Under UV-Irradiation. *IOP Conf. Ser.: Mater. Sci. Eng.* **2021**, *1011*, 012055, doi:10.1088/1757-899X/1011/1/012055.
34. Ariza-Tarazona, M.C.; Villarreal-Chiu, J.F.; Hernández-López, J.M.; Rivera De la Rosa, J.; Barbieri, V.; Siligardi, C.; Cedillo-González, E.I. Microplastic Pollution Reduction by a Carbon and Nitrogen-Doped TiO<sub>2</sub>: Effect of PH and Temperature in the Photocatalytic Degradation Process. *Journal of Hazardous Materials* **2020**, *395*, 122632, doi:10.1016/j.jhazmat.2020.122632.
35. Llorente-García, B.E.; Hernández-López, J.M.; Zaldívar-Cadena, A.A.; Siligardi, C.; Cedillo-González, E.I. First Insights into Photocatalytic Degradation of HDPE and LDPE Microplastics by a Mesoporous N-TiO<sub>2</sub> Coating: Effect of Size and Shape of Microplastics. *Coatings* **2020**, *10*, 658, doi:10.3390/coatings10070658.
36. Zhou, D.; Wang, L.; Zhang, F.; Wu, J.; Wang, H.; Yang, J. Feasible Degradation of Polyethylene Terephthalate Fiber-Based Microplastics in Alkaline Media with Bi<sub>2</sub>O<sub>3</sub>@N-TiO<sub>2</sub> Z-Scheme Photocatalytic System. *Advanced Sustainable Systems* **2022**, *6*, 2100516, doi:10.1002/adsu.202100516.

37. Yuwendi, Y.; Ibadurrohman, M.; Setiadi, S.; Slamet, S. Photocatalytic Degradation of Polyethylene Microplastics and Disinfection of E. Coli in Water over Fe- and Ag-Modified TiO<sub>2</sub> Nanotubes. *Bulletin of Chemical Reaction Engineering & Catalysis* **2022**, *17*, 263–277, doi:10.9767/bcrec.17.2.13400.263-277.

38. Zhou, D.; Luo, H.; Zhang, F.; Wu, J.; Yang, J.; Wang, H. Efficient Photocatalytic Degradation of the Persistent PET Fiber-Based Microplastics over Pt Nanoparticles Decorated N-Doped TiO<sub>2</sub> Nanoflowers. *Adv. Fiber Mater.* **2022**, *4*, 1094–1107, doi:10.1007/s42765-022-00149-4.

39. Zeng, H.; Xie, J.; Xie, H.; Su, B.-L.; Wang, M.; Ping, H.; Wang, W.; Wang, H.; Fu, Z. Bioprocess-Inspired Synthesis of Hierarchically Porous Nitrogen-Doped TiO<sub>2</sub> with High Visible-Light Photocatalytic Activity. *J. Mater. Chem. A* **2015**, *3*, 19588–19596, doi:10.1039/C5TA04649A.

40. Bradford, M.M. A Rapid and Sensitive Method for the Quantitation of Microgram Quantities of Protein Utilizing the Principle of Protein-Dye Binding. *Analytical Biochemistry* **1976**, *72*, 248–254, doi:10.1016/0003-2697(76)90527-3.

41. Telford, A.M.; Pham, B.T.T.; Neto, C.; Hawkett, B.S. Micron-Sized Polystyrene Particles by Surfactant-Free Emulsion Polymerization in Air: Synthesis and Mechanism. *Journal of Polymer Science Part A: Polymer Chemistry* **2013**, *51*, 3997–4002, doi:10.1002/pola.26841.

42. Napper, I.E.; Bakir, A.; Rowland, S.J.; Thompson, R.C. Characterisation, Quantity and Sorptive Properties of Microplastics Extracted from Cosmetics. *Marine Pollution Bulletin* **2015**, *99*, 178–185, doi:10.1016/j.marpolbul.2015.07.029.

43. Domínguez-Jaimes, L.P.; Cedillo-González, E.I.; Luévano-Hipólito, E.; Acuña-Bedoya, J.D.; Hernández-López, J.M. Degradation of Primary Nanoplastics by Photocatalysis Using Different Anodized TiO<sub>2</sub> Structures. *Journal of Hazardous Materials* **2021**, *413*, 125452, doi:10.1016/j.jhazmat.2021.125452.

44. Chamas, A.; Moon, H.; Zheng, J.; Qiu, Y.; Tabassum, T.; Jang, J.H.; Abu-Omar, M.; Scott, S.L.; Suh, S. Degradation Rates of Plastics in the Environment. *ACS Sustainable Chem. Eng.* **2020**, *8*, 3494–3511, doi:10.1021/acssuschemeng.9b06635.

45. Zhang, J.; Zhou, P.; Liu, J.; Yu, J. New Understanding of the Difference of Photocatalytic Activity among Anatase, Rutile and Brookite TiO<sub>2</sub>. *Phys. Chem. Chem. Phys.* **2014**, *16*, 20382–20386, doi:10.1039/C4CP02201G.

46. Ye, J.; Liu, W.; Cai, J.; Chen, S.; Zhao, X.; Zhou, H.; Qi, L. Nanoporous Anatase TiO<sub>2</sub> Mesocrystals: Additive-Free Synthesis, Remarkable Crystalline-Phase Stability, and Improved Lithium Insertion Behavior. *J. Am. Chem. Soc.* **2011**, *133*, 933–940, doi:10.1021/ja108205q.

47. Fujishima, A.; Zhang, X.; Tryk, D.A. TiO<sub>2</sub> Photocatalysis and Related Surface Phenomena. *Surface Science Reports* **2008**, *63*, 515–582, doi:10.1016/j.surrep.2008.10.001.

48. Rodríguez, E.M.; Márquez, G.; Tena, M.; Álvarez, P.M.; Beltrán, F.J. Determination of Main Species Involved in the First Steps of TiO<sub>2</sub> Photocatalytic Degradation of Organics with the Use of Scavengers: The Case of Ofloxacin. *Applied Catalysis B: Environmental* **2015**, *178*, 44–53, doi:10.1016/j.apcatb.2014.11.002.

49. Kik, K.; Bukowska, B.; Sicińska, P. Polystyrene Nanoparticles: Sources, Occurrence in the Environment, Distribution in Tissues, Accumulation and Toxicity to Various Organisms. *Environmental Pollution* **2020**, *262*, 114297, doi:10.1016/j.envpol.2020.114297.

50. Vital-Grappin, A.D.; Ariza-Tarazona, M.C.; Luna-Hernández, V.M.; Villarreal-Chiu, J.F.; Hernández-López, J.M.; Siligardi, C.; Cedillo-González, E.I. The Role of the Reactive Species Involved in the Photocatalytic Degradation of HDPE Microplastics Using C,N-TiO<sub>2</sub> Powders. *Polymers* **2021**, *13*, 999, doi:10.3390/polym13070999.

51. Socrates, G. *Infrared and Raman Characteristic Group Frequencies: Tables and Charts*; 3rd.; John Wiley & Sons: Hoboken, NJ, USA, 2004; ISBN 978-0-470-09307-8.

52. Park, C.H.; Lee, C.M.; Choi, J.W.; Park, G.C.; Joo, J. Enhanced Photocatalytic Activity of Porous Single Crystal TiO<sub>2</sub>/CNT Composites by Annealing Process. *Ceramics International* **2018**, *44*, 1641–1645, doi:10.1016/j.ceramint.2017.10.086.

**Disclaimer/Publisher's Note:** The statements, opinions and data contained in all publications are solely those of the individual author(s) and contributor(s) and not of MDPI and/or the editor(s). MDPI and/or the editor(s) disclaim responsibility for any injury to people or property resulting from any ideas, methods, instructions or products referred to in the content.